

Accelerated Recovery with RIS: Designing Wireless Resilience in Mission-Critical Environments

Kevin Weinberger*, Robert-Jeron Reifert*, Aydin Sezgin* and Mehdi Bennis†

*Institute of Digital Communication Systems, Ruhr University Bochum, Germany

†Centre for Wireless Communications, University of Oulu, Finland

Email: {kevin.weinberger,robert-.reifert,aydin.sezgin}@rub.de, mehdi.bennis@oulu.fi

Abstract—As 6G and beyond redefine connectivity, wireless networks become the foundation of critical operations, making resilience more essential than ever. With this shift, wireless systems cannot only take on vital services previously handled by wired infrastructures but also enable novel innovative applications that would not be possible with wired systems. As a result, there is a pressing demand for strategies that can adapt to dynamic channel conditions, interference, and unforeseen disruptions, ensuring seamless and reliable performance in an increasingly complex environment. Despite considerable research, existing resilience assessments lack comprehensive key performance indicators (KPIs), especially those quantifying its adaptability, which are vital for identifying a system’s capacity to rapidly adapt and reallocate resources. In this work, we bridge this gap by proposing a novel framework that explicitly quantifies the adaption performance by augmenting the gradient of the system’s rate function. To further enhance the network resilience, we integrate Reconfigurable Intelligent Surfaces (RISs) into our framework due to their capability to dynamically reshape the propagation environment while providing alternative channel paths. Numerical results show that gradient augmentation enhances resilience by improving adaptability under adverse conditions while proactively preparing for future disruptions.

I. INTRODUCTION

Future 6G networks are being shaped by recent advancements and global research, aiming to support both human-centric and artificial intelligence (AI)-driven applications with seamless connectivity [1]. This evolution envisions the realization of emerging applications such as autonomous transportation, remote-controlled robotics, and smart power grids. In these cases, even a brief network failure could lead to severe consequences, from safety hazards to operational breakdowns. It follows, that the network must not just support connectivity but also exhibit adaptive, context-aware, and autonomous behaviors. Interestingly, despite these challenges, much of the current research on 5G and 6G has focused primarily on reliability and robustness [2, 3], with less attention given to overall resilience—the ability to adapt and recover quickly from failures [4]. In fact, resilience encompasses a multitude

This work was supported in part by the German Research Foundation (DFG) in the course of the project SPP2433 under the project no. 541021107 (Measurement Technology on Flying Platforms) under grant SE 1697/22-1. This work was supported in part by the German Federal Ministry of Education and Research (BMBF) in the course of the 6GEM Research Hub under grant 16KISK037.

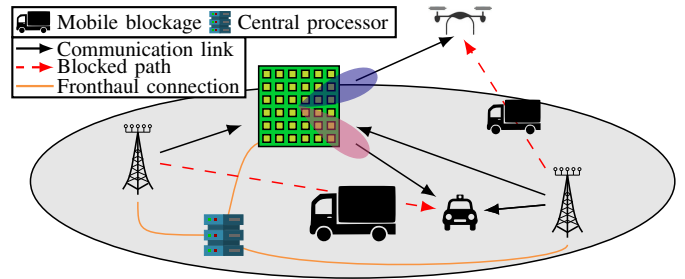


Figure 1. System model with mission-critical communications where mobile blockages can block the direct AP-user paths within the coherence interval

of aspects, by demanding the network to not only absorb disturbances and ensure operational stability but also to integrate adaptive mechanisms that enable autonomous recovery, or even thrive [5], from unexpected challenges [6, 7],

Despite extensive research efforts, current resilience assessments in wireless networks still lack comprehensive key performance indicators (KPIs) [8]. Particularly those that quantify adaptability, which is critical for evaluating a system’s ability to rapidly adapt and efficiently reallocate resources in changing conditions.

To bridge this gap, we propose a novel framework that explicitly quantifies adaptability by augmenting the gradient of the system’s rate function. The augmented gradient quantifies network responsiveness, enabling a balanced trade-off between robustness and adaptability. Our unified approach ensures stability during prolonged disruptions while swiftly adapting to sudden changes, enhancing service continuity and quality even when suffering from unexpected failures.

To implement our approach, resource allocation in the network must be supported by the active modification of radio channels. To this end, we integrate reconfigurable intelligent surfaces (RISs) into our design [9, 10]. With their ability to dynamically reconfigure the wireless propagation environment and establish alternative channel paths, RISs are shown to significantly enhance network resilience [11, 12]. In the following sections, we detail our methodology and present extensive numerical results that validate the effectiveness of our approach.

II. SYSTEM MODEL

This paper considers the RIS-aided cell-free multiple-input and multiple-output (MIMO) downlink system depicted in Fig 1. In details, a set of single-antenna users $\mathcal{K} = \{1, \dots, K\}$ is being served by a set of L -antenna access points (APs) $\mathcal{N} = \{1, \dots, N\}$. To enable an extra set of channel-links, we deploy an M -element RIS, configured as a uniform planar array, within user range. The position is chosen in a strategic way, so that the RIS is capable of providing alternative paths should direct links become blocked. The RIS and the APs are connected to and managed by a central processor (CP) via orthogonal fronthaul links. To meet the demands of the users, a quality-of-service (QoS) target is set as a desired data rate denoted as r_k^{des} , for each user.

A. Channel Model

The channel model in this paper assumes quasi-static block fading, where channel coefficients remain constant within the coherence time T_c but vary independently across coherence blocks. The direct channel link between AP n and user k is denoted as $\mathbf{h}_{n,k} \in \mathbb{C}^{L \times 1}$. The RIS-assisted reflected channel is given by $\mathbf{G}_{n,k} = \mathbf{H}_n \text{diag}(\mathbf{v}) \mathbf{g}_k \in \mathbb{C}^{L \times 1}$, where $\mathbf{H}_n \in \mathbb{C}^{L \times M}$ represents the AP-to-RIS link, $\mathbf{g}_k \in \mathbb{C}^{M \times 1}$ the RIS-to-user link, and $\text{diag}(\mathbf{v}) \in \mathbb{C}^{M \times M}$ the reflection coefficient matrix, with $\mathbf{v} = [v_1, v_2, \dots, v_M] \in \mathbb{C}^{M \times 1}$. Each reflection coefficient is defined as $v_m = e^{j\theta_m}$, where $\theta_m \in [0, 2\pi]$ is the phase shift at the m -th RIS element.

The aggregate direct channel vector for user k is given by $\mathbf{h}_k = [\mathbf{h}_{1,k}^T, \mathbf{h}_{2,k}^T, \dots, \mathbf{h}_{N,k}^T]^T \in \mathbb{C}^{NL \times 1}$, while the combined AP-to-RIS channel matrix is $\mathbf{H} = [\mathbf{H}_1^T, \mathbf{H}_2^T, \dots, \mathbf{H}_N^T]^T \in \mathbb{C}^{NL \times M}$. Similarly, the aggregate transmit signal vector is $\mathbf{x} = [\mathbf{x}_1^T, \mathbf{x}_2^T, \dots, \mathbf{x}_N^T]^T \in \mathbb{C}^{NL \times 1}$.

Using these aggregate representations, the received signal at user k is expressed as the sum of the direct and reflected channel components:

$$y_k = (\mathbf{h}_k + \mathbf{G}_k \mathbf{v})^H \mathbf{x} + n_k = (\mathbf{h}_k^{\text{eff}})^H \mathbf{x} + n_k, \quad (1)$$

where $\mathbf{G}_k = \mathbf{H} \text{diag}(\mathbf{g}_k)$, $\mathbf{h}_k^{\text{eff}} = \mathbf{h}_k + \mathbf{G}_k \mathbf{v}$ and $n_k \sim \mathcal{CN}(0, \sigma_k)$ represents the additive white Gaussian noise (AWGN).

The symbols intended to be decoded by user k are denoted by s_k . We assume these messages form an independent and identically distributed (i.i.d.) Gaussian codebook. The symbols for user k are transmitted by the n -th AP using the beamforming vector $\mathbf{w}_{n,k} \in \mathbb{C}^{L \times 1}$, both provided by the CP.

Hence, the overall transmit signal vector at the n -th AP is given as

$$\mathbf{x}_n = \sum_{k \in \mathcal{K}} \mathbf{w}_{n,k} s_k, \quad \forall n \in \mathcal{N}, \quad (2)$$

which is subject to the power constraint $\mathbb{E}\{\mathbf{x}_n^H \mathbf{x}_n\} \leq P_n^{\text{max}}$, that can be expressed as

$$\sum_{k \in \mathcal{K}} \|\mathbf{w}_{n,k}\|_2^2 \leq P_n^{\text{max}}, \quad \forall n \in \mathcal{N}. \quad (3)$$

The received signal (1) at user k is then given by

$$y_k = (\mathbf{h}_k^{\text{eff}})^H \mathbf{w}_{k,s_k} + \sum_{i \in \mathcal{K} \setminus \{k\}} (\mathbf{h}_k^{\text{eff}})^H \mathbf{w}_i s_i + n_k, \quad (4)$$

where the first term represents user k 's desired signal, and the second term accounts for all the other user's interference.

Thus, we formulate the signal-to-interference-plus-noise ratio (SINR) of user k decoding its message as

$$\Gamma_k = \frac{|(\mathbf{h}_k^{\text{eff}})^H \mathbf{w}_k|^2}{\sum_{i \in \mathcal{K} \setminus \{k\}} |(\mathbf{h}_k^{\text{eff}})^H \mathbf{w}_i|^2 + \sigma^2}, \quad (5)$$

where σ^2 denotes the noise power.

Using these definitions, each user's QoS demands is satisfied, if the following condition holds:

$$r_k^{\text{des}} \leq r_k \leq B \log_2(1 + \Gamma_k), \quad (6)$$

where B denotes the transmission bandwidth and r_k represents the allocated rate of user k .

When the direct links to user k are blocked, by denoting $\mathbf{h}_k^{\text{RIS}} = \mathbf{G}_k \mathbf{v}$, we can define the RIS-link SINR Γ_k^{RIS} and rate expressions r_k^{RIS} as

$$\Gamma_k^{\text{RIS}} = \frac{|(\mathbf{h}_k^{\text{RIS}})^H \mathbf{w}_k|^2}{\sum_{i \in \mathcal{K} \setminus \{k\}} |(\mathbf{h}_k^{\text{RIS}})^H \mathbf{w}_i|^2 + \sigma^2}, \quad (7)$$

$$r_k^{\text{RIS}} \leq B \log_2(1 + \Gamma_k^{\text{RIS}}), \quad (8)$$

which effectively represents the case, in which user k is only served over the RIS-assisted links. Since we quantify the network's adaptability with the rate's gradient, by denoting $\mathbf{a}_{k,i} = \mathbf{v}^H \mathbf{G}_k^H \mathbf{w}_i$ and $\mathbf{b}_{k,i} = \mathbf{w}_i^H \mathbf{G}_k \mathbf{v} \mathbf{G}_k^H \mathbf{w}_i \in \mathbb{C}^{M \times 1}$ we can express the gradient of the RIS-link rate with respect to (w.r.t.) the phase shifts as

$$\nabla_{\mathbf{v}} r_k^{\text{RIS}} = \frac{2B(\mathbf{b}_{k,k} - \Gamma_k^{\text{RIS}} \mathbf{b}_{k,i})}{\ln(2)(\sum_{i \in \mathcal{K}} |\mathbf{a}_{k,i}|^2 + \sigma^2)}. \quad (9)$$

Proof: For a detailed derivation, we refer to Appendix A

III. RIS IN THE CONTEXT OF RESILIENCE

A. Resilience Metric

In the context of resilience, wireless networks must maintain reliable performance even under dynamic conditions, such as link blockages or resource fluctuations. To ensure this, the network operates with a predefined target throughput dictated by the QoS requirements, where r_k^{des} represents user k 's desired QoS level. These QoS demands remain constant within the coherence interval, while the network's sum throughput varies based on allocated resources at time t , expressed as $\sum_{k=1}^K r_k(t)$, where $r_k(t)$ denotes the allocated data rate for user k at time t . To characterize resilience behavior, we define two key moments in time: t_0 , denoting the initial time when degradation manifests, and t_q denoting the time at which the system reaches a recovered state. Building on the resilience metric proposed in [6], we adopt the network's absorption, adaptation, and time-to-recovery metrics as cornerstones of the

resilience performance. More precisely, the absorption metric is given by

$$r_{\text{abs}} = \frac{1}{K} \sum_{k \in \mathcal{K}} \frac{r_k(t_0)}{r_k^{\text{des}}}, \quad (10)$$

which quantifies the system's ability to sustain performance when facing disruptions. The adaptation metric, expressed as

$$r_{\text{ada}} = \frac{1}{K} \sum_{k \in \mathcal{K}} \frac{r_k(t_q)}{r_k^{\text{des}}}, \quad (11)$$

captures how well the network recovers. Finally, the time-to-recovery metric measures the speed of resilience and is given by

$$r_{\text{rec}} = \begin{cases} 1, & \text{if } t_q - t_0 \leq T_0 \\ \frac{T_0}{t_q - t_0}, & \text{otherwise.} \end{cases} \quad (12)$$

where, T_0 represents the desired recovery time, defining the duration for which a functionality degradation is considered tolerable. A linear combination of the equations (10)-(12) defines the considered resilience metric as

$$r = \lambda_1 r_{\text{abs}} + \lambda_2 r_{\text{ada}} + \lambda_3 r_{\text{rec}}, \quad (13)$$

where the fixed weights λ_i , for $i \in \{1, 2, 3\}$, reflect the network operator's priorities, such as emphasizing robustness, adaptation quality, or recovery time. These non-negative weights satisfy $\sum_{i=1}^3 \lambda_i = 1$, ensuring that the best-case resilience value is $r = 1$.

B. RIS as Resiliency Mechanism

As previously discussed, an effective resiliency mechanism should promptly and efficiently address disruptions. However, outages arise for various reasons, each with different severities and impacts on the system. In this work, we propose leveraging the RIS to enhance resilience. More precisely, integrating the RIS introduces alternative reconfigurable channel paths to each user. Even when direct paths from all APs to a user are entirely obstructed, the system can still recover by leveraging RIS-assisted paths. In fact, without these alternative paths, communication with a blocked user could fail entirely in the presence of disruptions beyond the system's capacity to mitigate. In terms of the resilience metric, the inherent redundancy that the RIS links contribute to the system can also be utilized to increase robustness [13]. Additionally, the reconfigurability of the phase shifts at the RIS provides the system with an extra degree of freedom, which enables more effective rerouting of the signal in case of blockages. This translates to the RIS aiding in adapting quicker to disturbances, improving adaption performance r_{ada} , while also decreasing the time-to-recovery r_{rec} [11]. This becomes an essential characteristic, especially when the resilience actions must restore system performance within a short desired recovery time T_0 . To this end, we propose to quantify this property by introducing the rate gradient $\nabla_{\mathbf{v}} r_k^{\text{RIS}}$ as a key metric. Maximizing its norm enhances user rate sensitivity, allowing rapid adaptation to disruptions like total line-of-sight (LoS) loss. As a result, the RIS enables

balancing of both, redundancy and adaptability by providing redundant paths and reconfigurable phase shifts, respectively.

IV. PROBLEM FORMULATION

To analyze the impact of the RIS on resilience performance, we formulate a multi-objective optimization problem that provides precise control over the individual components of the resilience metric. Furthermore, we propose to optimize this problem not only *during* the recovery phase, but also *before* any blockage occurs. The objective is to enable enhanced recovery from disturbances while simultaneously fortifying the system against future failures. The inclusion of multiple objectives is motivated by the versatility introduced through the weight parameters λ_i in (13), which determine the relative emphasis placed on each aspect of the metric. First, we intend to capture the adaption metric r_{ada} by considering the network wide adaption gap [6, 11] $\Psi = \sum_{k \in \mathcal{K}} \left| \frac{r_k}{r_k^{\text{des}}} - 1 \right|$, which represents the overall goal of serving each user with its required QoS. Second, we employ gradient augmentation to enhance adaption performance, which boosts both, the time-to-recovery r_{rec} as well as the adaption r_{ada} . This is achieved by maximizing the norm of the gradient of the RIS-assisted rate w.r.t. the phase shift vectors $\|\nabla_{\mathbf{v}} r_k^{\text{RIS}}\|_2$. Third, we provide robustness by including a RIS-link-redundancy term, represented by the difference between the total rate and the RIS-only rate as $\Delta_k^{\text{RIS}} = |r_k - r_k^{\text{RIS}}|^2$. By reducing this term we facilitate that some portion of the received signal at user k is routed through the RIS-assisted links. With the above considerations, the overall problem can be formulated as

$$\min_{\mathbf{w}, \mathbf{v}, \mathbf{r}} \quad \nu_{\text{const}} \Psi - \sum_{k \in \mathcal{K}} \alpha_{1,k} \|\nabla_{\mathbf{v}} r_k^{\text{RIS}}\|_2 + \sum_{k \in \mathcal{K}} \alpha_{2,k} \Delta_k \quad (\text{P1})$$

$$\text{s.t.} \quad (3),$$

$$r_k \leq B \log_2(1 + \Gamma_k), \quad \forall k \in \mathcal{K}, \quad (14)$$

$$r_k^{\text{RIS}} \leq B \log_2(1 + \Gamma_k^{\text{RIS}}), \quad \forall k \in \mathcal{K}, \quad (15)$$

$$|v_m| = 1, \quad \forall m \in \{1, \dots, M\}, \quad (16)$$

where $\mathbf{r} = [r_1, r_2, \dots, r_K, r_1^{\text{RIS}}, r_2^{\text{RIS}}, \dots, r_K^{\text{RIS}}]^T$ represents the stacked rate vector, and the unit modulus constraints in (16) enforce the phase shift conditions $0 \leq \theta_m \leq 2\pi, \forall m \in \{1, \dots, M\}$. The weight ν_{const} is set to a very high value to ensure that the adaptation gap Ψ always takes priority, while $\alpha_{1,k}$ and $\alpha_{2,k}$ enable versatility in designing the adaptability-robustness trade-off for each user individually. Additionally, this approach enables efficient resource allocation so that users that are mission-critical or in vulnerable states become more resilient against failures.

Solving problem (P1) is complex due to the interdependence between the variables \mathbf{w} and \mathbf{v} in $\nabla_{\mathbf{v}} r_k^{\text{RIS}}$, as well as the constraints (14) and (15). Further minimizing the norm of the gradient and satisfying the unit modulus constraint are additional challenges, especially when coupled with the rate constraints in (14) and (15). These elements together make the optimization problem non-trivial, requiring specialized techniques such as alternating optimization and successive convex approximations (SCAs) to handle these interdependencies

effectively [10]. In fact, both sub-problems can be efficiently solved within the same SCA framework [10]. As a result, full convergence of one sub-problem is not required before moving to the other; instead, just one iteration of each sub-problem can be performed before switching to the other. This approach significantly accelerates the overall convergence process, which is crucial in resilience scenarios and allows the evaluation of the resilience performance without the need to converge [11].

A. Beamforming Design

As a result of the alternating optimization approach, the phase shifters \mathbf{v} are assumed to be fixed for the duration of the beamforming design. Thus, problem (P1) can be written as

$$\min_{\mathbf{w}, \mathbf{r}, \mathbf{q}, \mathbf{u}} \nu_{\text{const}} \Psi - \sum_{k \in \mathcal{K}} \alpha_{1,k} u_k + \sum_{k \in \mathcal{K}} \alpha_{2,k} \Delta_k \quad (\text{P2})$$

s.t. (3),

$$r_k \leq B \log_2(1 + q_k), \quad \forall k \in \mathcal{K}, \quad (17)$$

$$r_k^{\text{RIS}} \leq B \log_2(1 + q_k^{\text{RIS}}), \quad \forall k \in \mathcal{K}, \quad (18)$$

$$q_k \leq \Gamma_k, \quad \forall k \in \mathcal{K}, \quad (19)$$

$$q_k^{\text{RIS}} \leq \Gamma_k^{\text{RIS}}, \quad \forall k \in \mathcal{K}, \quad (20)$$

$$u_k \leq \sum_{k \in \mathcal{K}} \|\nabla_{\mathbf{v}} r_k^{\text{RIS}}\|_2, \quad \forall k \in \mathcal{K}, \quad (21)$$

$$\mathbf{q} \geq 0, \mathbf{u} \geq 0 \quad (22)$$

where the introduction of the slack variables $\mathbf{q} = [q_1, \dots, q_K, q_1^{\text{RIS}}, \dots, q_K^{\text{RIS}}]$ convexify the rate expressions for the effective and RIS-link and the slack variables $\mathbf{u} = [u_1, \dots, u_K]$ linearize the norm in the objective function. Furthermore, (22) signifies that all values in \mathbf{q} , and also \mathbf{u} , are nonnegative. However, the constraints in (19)-(21) remain non-convex but can be rendered in a convex form through the SCA approach. To this end, we rewrite (19) as

$$\sum_{i \in \mathcal{K} \setminus \{k\}} |(\mathbf{h}_k^{\text{eff}})^H \mathbf{w}_i|^2 + \sigma^2 - \frac{|(\mathbf{h}_k^{\text{eff}})^H \mathbf{w}_k|^2}{q_k} \leq 0. \quad (23)$$

By applying the first-order Taylor approximation around the point $(\tilde{\mathbf{w}}, \tilde{q})$ to the fractional term, we obtain the following convex approximation of (23) [10]

$$\sum_{i \in \mathcal{K} \setminus \{k\}} |(\mathbf{h}_k^{\text{eff}})^H \mathbf{w}_i|^2 + \sigma^2 + \frac{|(\mathbf{h}_k^{\text{eff}})^H \tilde{\mathbf{w}}_k|^2}{(\tilde{q}_k)^2} q_k - \frac{2 \text{Re}\{\tilde{\mathbf{w}}_k^H (\mathbf{h}_k^{\text{eff}})^H (\mathbf{h}_k^{\text{eff}})^H \mathbf{w}_k\}}{\tilde{q}_k} \leq 0, \forall k \in \mathcal{K}. \quad (24)$$

Due to the same structure, the same process can be repeated for the RIS-link SINR in (20), by substituting $\mathbf{h}_k^{\text{eff}}$ with $\mathbf{h}_k^{\text{RIS}}$ and q_k with q_k^{RIS} , respectively:

$$\sum_{i \in \mathcal{K} \setminus \{k\}} |(\mathbf{h}_k^{\text{RIS}})^H \mathbf{w}_i|^2 + \sigma^2 + \frac{|(\mathbf{h}_k^{\text{RIS}})^H \tilde{\mathbf{w}}_k|^2}{(\tilde{q}_k^{\text{RIS}})^2} q_k - \frac{2 \text{Re}\{\tilde{\mathbf{w}}_k^H (\mathbf{h}_k^{\text{RIS}})^H (\mathbf{h}_k^{\text{RIS}})^H \mathbf{w}_k\}}{\tilde{q}_k^{\text{RIS}}} \leq 0, \forall k \in \mathcal{K}. \quad (25)$$

Utilizing the homogeneity property of norms, the constraint in (21) can also be reformulated in a similar structure

$$\ln(2) \left(\sum_{i \in \mathcal{K}} |a_{k,i}|^2 + \sigma^2 \right) - \frac{2B \|\mathbf{b}_{k,k} - q_k^{\text{RIS}} \sum_{i \in \mathcal{K} \setminus \{k\}} \mathbf{b}_{k,i}\|_2}{u_k} \leq 0, \quad \forall k \in \mathcal{K}, \quad (26)$$

where the fraction can be linearized by a Taylor approximation around the point $(\tilde{\mathbf{w}}, \tilde{q}, \tilde{u})$ as

$$T_k^w = \beta_k \|\boldsymbol{\eta}_k\| - \frac{\beta_k}{\tilde{u}_k} \|\boldsymbol{\eta}_k\| (u_k - \tilde{u}_k) + \frac{\beta_k}{\|\boldsymbol{\eta}_k\|} \left(-\text{Re}\{\boldsymbol{\eta}^H \sum_{i \in \mathcal{K} \setminus \{k\}} (\mathbf{b}_{k,i})\} (q_k^{\text{RIS}} - \tilde{q}_k^{\text{RIS}}) + \text{Re}\{\boldsymbol{\eta}^H (\boldsymbol{\Omega}_{k,k}^a + \boldsymbol{\Omega}_{k,k}^b) (\mathbf{w}_k - \tilde{\mathbf{w}}_k)\} - \sum_{i \in \mathcal{K} \setminus \{k\}} \text{Re}\{\boldsymbol{\eta}^H (\tilde{q}_k^{\text{RIS}} (\boldsymbol{\Omega}_{k,i}^a + \boldsymbol{\Omega}_{k,i}^b)) (\mathbf{w}_i - \tilde{\mathbf{w}}_i)\} \right), \quad (27)$$

where $\beta_k = \frac{2B}{\tilde{u}_k}$, $\boldsymbol{\eta}_k = \tilde{\mathbf{b}}_{k,k} - \tilde{q}_k \sum_{i \in \mathcal{K} \setminus \{k\}} \tilde{\mathbf{b}}_{k,i}$, $\boldsymbol{\Omega}_{k,i}^a = \mathbf{w}_i^H \mathbf{G}_k \mathbf{v} \mathbf{G}_k^H$ and $\boldsymbol{\Omega}_{k,i}^b = \mathbf{G}_k^H \mathbf{w}_i (\mathbf{G}_k \mathbf{v})^H$. Thus, the approximation of problem (P2) can be written as

$$\min_{\mathbf{w}, \mathbf{r}, \mathbf{q}, \mathbf{u}} \nu_{\text{const}} \Psi - \alpha_{1,k} u_k + \sum_{k \in \mathcal{K}} \alpha_{2,k} \Delta_k \quad (\text{P2.1})$$

s.t. (3), (17), (18), (22), (24), (25),

$$\ln(2) \left(\sum_{i \in \mathcal{K}} |a_{k,i}|^2 + \sigma^2 \right) - T_k^w \leq 0, \forall k \in \mathcal{K}. \quad (28)$$

Problem (P2.1) is convex and can be solved iteratively using the SCA method. More precisely, we denote $\boldsymbol{\Lambda}_z^w = [\mathbf{w}_z^T, \boldsymbol{\kappa}_z^T]^T$ as a vector stacking the optimization variables of the beamforming design problem at iteration z , where $\boldsymbol{\kappa}_z = [\mathbf{r}_z^T, \mathbf{q}_z^T, \mathbf{u}_z^T]^T$. Similarly $\tilde{\boldsymbol{\Lambda}}_z^w = [\tilde{\mathbf{w}}_z^T, \tilde{\boldsymbol{\kappa}}_z^T]^T$ and $\hat{\boldsymbol{\Lambda}}_z^w = [\hat{\mathbf{w}}_z^T, \hat{\boldsymbol{\kappa}}_z^T]^T$ define the optimal solutions and the point, around which the approximations are computed, respectively. With these expressions, given a point $\hat{\boldsymbol{\Lambda}}_z^w$, an optimal solution $\tilde{\boldsymbol{\Lambda}}_z^w$ can be obtained by solving problem (P2.1).

B. Phase Shift Design

While designing the phase shifters at the RIS, the beamformers are assumed to be fixed due to the alternating optimization approach. With the goal of using a comparable problem structure as in (P2), we denote $|(\mathbf{h}_k^{\text{eff}})^H \mathbf{w}_k|^2 = \tilde{h}_{i,k} + \tilde{\mathbf{G}}_{i,k} \mathbf{v}$, where $\tilde{h}_{i,k} = \mathbf{w}_k^H \mathbf{h}_i$ and $\tilde{\mathbf{G}}_{i,k} = \mathbf{w}_k^H \mathbf{G}_i$. With the above definitions, the SINR constraints can be written similar to (23) as

$$\sum_{i \in \mathcal{K} \setminus \{k\}} |\tilde{h}_{k,i} + \tilde{\mathbf{G}}_{k,i} \mathbf{v}|^2 + \sigma^2 - \frac{|(\tilde{h}_{k,k} + \tilde{\mathbf{G}}_{k,k} \mathbf{v})|^2}{q_k} \leq 0, \quad (29)$$

$$\sum_{i \in \mathcal{K} \setminus \{k\}} |\mathbf{G}_{k,i} \mathbf{v}|^2 + \sigma^2 - \frac{|(\mathbf{G}_{k,k} \mathbf{v})|^2}{q_k} \leq 0, \forall k \in \mathcal{K}. \quad (30)$$

By applying the same procedure used to obtain equations (24) and (25), the Taylor approximations for the SINR constraints around the phase shift vector \mathbf{v} instead of \mathbf{w} can be derived [10, 11]. Regarding the gradient-norm constraint in (21), we

utilize the reformulation in (26) and calculate the linearization around the point $(\tilde{v}, \tilde{q}, \tilde{u})$ as

$$T_k^v = \beta_k \|\boldsymbol{\eta}_k\| - \frac{\beta_k}{\tilde{u}_k} \|\boldsymbol{\eta}_k\| (u_k - \tilde{u}_k) + \frac{\beta_k}{\|\boldsymbol{\eta}_k\|} \left(-\text{Re}\{\boldsymbol{\eta}^H \sum_{i \in \mathcal{K} \setminus \{k\}} (\tilde{\mathbf{b}}_{k,i})\} (q_k^{\text{RIS}} - \tilde{q}_k^{\text{RIS}}) + \text{Re}\{\boldsymbol{\eta}^H (\mathbf{S}_{k,k} - q_k^{\text{RIS}} \sum_{i \in \mathcal{K} \setminus \{k\}} \mathbf{S}_{k,i}) (\mathbf{v}_k - \tilde{\mathbf{v}}_k)\} \right), \quad (31)$$

where $\mathbf{S}_{k,i} = 2\mathbf{G}_k^H \mathbf{w}_i \mathbf{w}_i^H \mathbf{G}_k$. For the unit-modulus constraint in (16), we adopt the penalty method [11]. Hence, the weighted first-order Taylor approximation of the term $\sum_{m=1}^M (|v_m|^2 - 1)$, which is given by $\Phi = \alpha_v \sum_{m=1}^M \text{Re}\{2\tilde{v}_m^* v_m - |\tilde{v}_m|^2\}$ is included as a penalty in the objective function, where α_v is a weighting factor. At this point, the approximated optimization problem for the phase shift design can be formulated as

$$\min_{\mathbf{v}, \mathbf{r}, \mathbf{q}, \mathbf{u}} \nu_{\text{const}} \Psi + \Phi - \alpha_{1,k} u_k + \sum_{k \in \mathcal{K}} \alpha_{2,k} \Delta_k \quad (\text{P3})$$

$$\text{s.t.} \quad (17), (18), (22), (\widetilde{29}), (\widetilde{30}),$$

$$\ln(2) \left(\sum_{i \in \mathcal{K}} |a_{k,i}|^2 + \sigma^2 \right) - T_k^v \leq 0, \forall k \in \mathcal{K}. \quad (32)$$

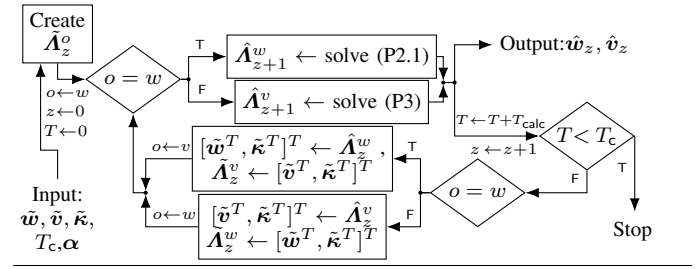
where $(\widetilde{29}), (\widetilde{30})$ are the first-order Taylor approximation of (29) and (30) around the point $(\tilde{v}, \tilde{q}, \tilde{u})$, respectively.¹ Due to the similarity of the problem formulation and the utilization of the same SCA framework, problem (P3) can be solved by defining $\mathbf{A}_z^v = [\mathbf{v}_z^T, \boldsymbol{\kappa}_z^T]^T$ and following the same iterative procedure as for solving problem (P2.1).

C. Resilience-Guided Alternating Optimization

In the context of resilience, our goal is to find a solution that meets a specific trade-off defined by the weights $\lambda_i, \forall i \in \{1, 2, 3\}$ in (13). At the same time, we want the system to adapt to failures quickly. Therefore, instead of fully optimizing each sub-problem until convergence, we perform just one iteration for each sub-problem before switching to the other [11]. This is only possible because the same framework is used to solve both sub-problems, which helps us reduce the adaptation gap more rapidly. Once the adaptation gap converges, the algorithm then enhances adaptability and robustness to prepare for future failures while keeping the gap minimized. By choosing the weights $\boldsymbol{\alpha} = [\alpha_{1,1}, \dots, \alpha_{1,K}, \alpha_{2,1}, \dots, \alpha_{2,K}]$ accordingly, the algorithm can be tailored to respond effectively to different values of λ_i . The detailed steps of the resilience-guided alternating optimization are presented in Algorithm 1, where T_{calc} is the time needed to compute the solution of a sub-problem and T_c is the coherence time.

¹Due to the similarity to the beamforming design problem and for page length constraints reasons, the derivation of these equations is omitted.

Algorithm 1 Resiliency-aware Alternating Optimization



V. NUMERICAL RESULTS

In this section, we numerically evaluate the performance of our proposed gradient augmentation approach in the context of resilience. To this end we assume a cell-free MIMO system with $N = 2$ AP, each of which equipped with $L = 8$ antennas and positioned on opposite corners of the area, which spans $[-500, 500] \times [-500, 500] \text{m}^2$. We assume $K = 6$ single-antenna users to be distributed equally on a circle with a radius of 250m around the RIS, which is centrally positioned and consists of $M = 500$ reflective elements arranged in a quadratic grid with $\lambda_f/4$ spacing, where $\lambda_f = 0.1\text{m}$ is the wavelength. For the RIS channels, we use the correlated channel model from [14]. Further, reflected channels follow a line-of-sight model, while direct channels experience Rayleigh fading with log-normal shadowing (8dB standard deviation). Moreover, we assume a bandwidth of $B = 10\text{MHz}$, a noise power of $\sigma^2 = -100\text{dBm}$, a maximum transmit power of $P_n^{\text{max}} = 32\text{dBm}$, $T_0 = 0.15\text{s}$ and each user to request a QoS of $r_k^{\text{des}} = 6\text{Mbps}$. We define an outage as the event where each direct link between AP n and user k is subject to a blockage, removing it from the network. RIS-assisted links are exempt, as the RIS is positioned to bypass potential blockages, ensuring an unobstructed communication path. Additionally, blockages are considered from the strongest channel onward to force reoptimization, as this approach highlights the most significant impact on network's performance and resilience capability. Regarding the weights $\boldsymbol{\alpha}$, we employ a metric that weights the users based on their direct channel strengths, i.e., $\alpha_{1/2,k} = \frac{\|\mathbf{h}_k\|}{\max_{i \in \mathcal{K}} \|\mathbf{h}_i\|} \in [0, 1]$.

Fig. 2 displays the adaption performance r_{ada} for the proposed framework, which also maximizes the network's adaptability and compares it with the adaption performance of the baseline method proposed in [11], which only optimizes the adaption gap Ψ . In addition, we include the robustness-only case in which $\alpha_{1,k} = 0, \forall k \in \mathcal{K}$. The figure shows the significant increase in adaption performance of the proposed framework when compared to the baseline method. The results show that the proposed framework recovers from three consecutive blockages not only more quickly but also at a higher value than the other methods, utilizing the same resources. This demonstrates the effectiveness of gradient augmentation in the context of resilience. The figure also illustrates that prioritizing robustness alone can actually degrade absorption performance due to the resource overhead required to ensure full redundant network coverage via RIS-assisted paths only. This underscores the need to balance adaptability and robustness in resilience

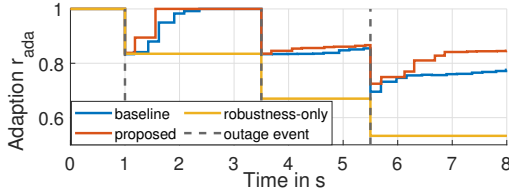


Figure 2. Adaption performance of the proposed gradient-augmentation approach, the baseline adaption gap-only and the robustness-only approach

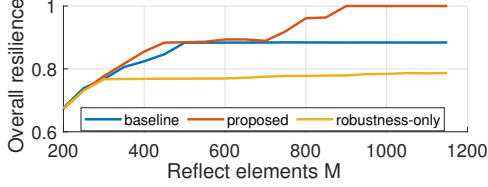


Figure 3. Overall resilience r for the second blockage over the number of reflecting elements M for the proposed, baseline and robustness-only approach

design, as shown in Fig. 3, which presents the overall resilience (13) for the second blockage over different numbers of reflect elements M with $\lambda_1 = \lambda_2 = \lambda_3 = \frac{1}{3}$. The figure reveals distinct scaling behaviors among the three approaches. For $M < 300$, resources are insufficient to meet user rate demands even pre-blockage. Beyond $M = 300$, robustness-only scaling declines as using RIS paths only for redundancy becomes inefficient. In contrast, the adaption-based methods utilize resources more effectively, scaling until $M \approx 500$, where they are able to fully recover from the first blockage. The proposed method with optimized adaptability achieves this earlier at $M = 450$ due to faster resource reallocation enabled by gradient augmentation. At $M = 700$, the proposed method begins to scale towards optimal resilience $r = 1$, while the baseline stops scaling, struggling with reoptimization and suffering from absorption r_{abs} and time-to-recovery r_{rec} penalties.

VI. CONCLUSION

As wireless networks play a vital role in critical services, resilience becomes a crucial property, requiring not only robustness but also adaptability to react to unforeseen disruptions. Traditional approaches often neglect this aspect, limiting their ability to sustain performance in dynamic environments. To address this, we introduced a framework that explicitly captures adaptability and integrates RISs to further improve resilience. Results show that by utilizing gradient augmentation while continuously reallocating resources, our method maintains high resilience even after consecutive blockages, outperforming the baseline strategy that degrades more rapidly. This underscores the efficient use of available resources in a dynamic environment, laying the groundwork for uninterrupted network performance in future wireless systems.

APPENDIX A

DERIVATION OF GRADIENT $\nabla_{\mathbf{v}} r_k$

Using the chain rule, we write the gradient of r_k^{RIS} in (8) as

$$\nabla_{\mathbf{v}} r_k^{\text{RIS}} = \frac{\partial r_k^{\text{RIS}}}{\partial \Gamma_k^{\text{RIS}}} \nabla_{\mathbf{v}} \Gamma_k^{\text{RIS}} = \frac{B}{\ln(2)} \frac{1}{1 + \Gamma_k^{\text{RIS}}} \nabla_{\mathbf{v}} \Gamma_k^{\text{RIS}}. \quad (33)$$

By denoting $\mathbf{h}_{k,i}^w = \mathbf{G}_k^H \mathbf{w}_i$ and $\eta_{k,i} = \mathbf{v}^H \mathbf{h}_{k,i}^w$, the RIS-only SINR Γ_k^{RIS} can be written as

$$\Gamma_k^{\text{RIS}} = \frac{|\eta_{k,k}|^2}{\sum_{i \in \mathcal{K} \setminus \{k\}} |\eta_{k,i}|^2 + \sigma^2} = \frac{N_{\Gamma_k}}{D_{\Gamma_k}}. \quad (34)$$

Applying the quotient rule, we arrive at

$$\begin{aligned} \nabla_{\mathbf{v}} \Gamma_k &= \frac{D_{\Gamma_k} \nabla_{\mathbf{v}} N_{\Gamma_k} - N_{\Gamma_k} \nabla_{\mathbf{v}} D_{\Gamma_k}}{D_{\Gamma_k}^2} = \frac{\nabla_{\mathbf{v}} N_{\Gamma_k} - \Gamma_k \nabla_{\mathbf{v}} D_{\Gamma_k}}{D_{\Gamma_k}}, \\ \nabla_{\mathbf{v}} N_{\Gamma_k} &= 2 \mathbf{h}_{k,k}^w (\mathbf{h}_{k,k}^w)^H \mathbf{v}, \quad \nabla_{\mathbf{v}} D_{\Gamma_k} = 2 \sum_{i \in \mathcal{K} \setminus \{k\}} \mathbf{h}_{k,i}^w (\mathbf{h}_{k,i}^w)^H \mathbf{v}. \end{aligned} \quad (35)$$

By substituting (35) into (33) and simplifying $\frac{1}{1 + \Gamma_k} \frac{1}{D_{\Gamma_k}} = \frac{1}{D_{\Gamma_k} + N_{\Gamma_k}}$ we obtain

$$\nabla_{\mathbf{v}} r_k^{\text{RIS}} = \frac{2B (\mathbf{h}_{k,k}^w (\mathbf{h}_{k,k}^w)^H \mathbf{v} - \Gamma_k \sum_{i \in \mathcal{K} \setminus \{k\}} \mathbf{h}_{k,i}^w (\mathbf{h}_{k,i}^w)^H \mathbf{v})}{\ln(2) (N_{\Gamma_k} + D_{\Gamma_k})}. \quad (36)$$

By recognizing that $(\mathbf{h}_{k,i}^w)^H \mathbf{v}$ is a scalar, we can transform $\mathbf{h}_{k,k}^w (\mathbf{h}_{k,k}^w)^H \mathbf{v}$ into $(\mathbf{h}_{k,k}^w)^H \mathbf{v} \mathbf{h}_{k,k}^w$. This simplification facilitates further calculations in the paper, leading to equation (9).

REFERENCES

- [1] X. You, C.-X. Wang, J. Huang, X. Gao, Z. Zhang, M. Wang, Y. Huang, C. Zhang, Y. Jiang, J. Wang *et al.*, "Towards 6G wireless communication networks: Vision, enabling technologies, and new paradigm shifts," *Science China information sciences*, vol. 64, pp. 1–74, 2021.
- [2] M. Shafi, A. F. Molisch, P. J. Smith, T. Haustein, P. Zhu, P. De Silva, F. Tufvesson, A. Benjebbour, and G. Wunder, "5G: A tutorial overview of standards, trials, challenges, deployment, and practice," *IEEE Journal on Sel. Areas in Commun.*, vol. 35, no. 6, pp. 1201–1221, 2017.
- [3] S. Alraih, I. Shaya, M. Behjati, R. Nordin, N. F. Abdullah, A. Abu-Samah, and D. Nandi, "Revolution or evolution? Technical requirements and considerations towards 6G mobile communications," *Sensors*, vol. 22, no. 3, p. 762, 2022.
- [4] M. Najarian and G. J. Lim, "Design and assessment methodology for system resilience metrics," *Risk Anal.*, vol. 39, no. 9, pp. 1885–1898, 2019.
- [5] K. Weinberger and A. Sezgin, "Dynamic rate splitting grouping for antifragile responses to wireless network disruptions," in *ISWCS*, 2024.
- [6] R.-J. Reifert, S. Roth, A. A. Ahmad, and A. Sezgin, "Comeback kid: Resilience for mixed-critical wireless network resource management," *IEEE Trans. on Vehicul. Techn.*, vol. 72, no. 12, pp. 16 177–16 194, 2023.
- [7] R.-J. Reifert, Y. Karacora, C. Chaccour, A. Sezgin, and W. Saad, "Resilience and criticality: Brothers in arms for 6G," *arXiv preprint arXiv:2412.03661*, 2024.
- [8] N. H. Mahmood, S. Samarakoon, P. Porambage, M. Bennis, and M. Latva-aho, "Resilient-by-design: A resiliency framework for future wireless networks," 2024.
- [9] E. Basar, M. Di Renzo, J. De Rosny, M. Debbah, M.-S. Alouini, and R. Zhang, "Wireless communications through reconfigurable intelligent surfaces," *IEEE access*, vol. 7, pp. 116 753–116 773, 2019.
- [10] K. Weinberger, A. A. Ahmad, A. Sezgin, and A. Zappone, "Synergistic benefits in IRS- and RS-enabled C-RAN with energy-efficient clustering," *IEEE Trans. on Wirel. Commun.*, 2022.
- [11] K. Weinberger, R.-J. Reifert, A. Sezgin, and E. Basar, "RIS-enhanced resilience in cell-free MIMO," in *WSA and SCC*, 2023.
- [12] S. Sivadevuni, F. Lotfi, B. Ahmad, K. Weinberger, and A. Sezgin, "Preparing for the inevitable: Preventing outages using resilient RIS-assisted JCRAS," in *CAMSAP*, 2023, pp. 241–245.
- [13] Z. Li, H. Hu, J. Zhang, and J. Zhang, "RIS-assisted mmwave networks with random blockages: Fewer large RISs or more small RISs?" *IEEE Trans. on Wirel. Commun.*, vol. 22, no. 2, pp. 986–1000, 2023.
- [14] E. Björnson and L. Sanguinetti, "Rayleigh fading modeling and channel hardening for reconfigurable intelligent surfaces," *IEEE Wirel. Commun. Lett.*, vol. 10, no. 4, pp. 830–834, 2021.